Marta Lorenzon, Lucía Ruano Posada, Myrsini Gkouma, Liora Bouzaglou, Philip Ebeling, Alexander Fantalkin

From Earth to Eternity: Investigating Bitumen and Clay Use in Byzantine Church Construction at Ashdod-Yam

Archäologischer Anzeiger 2. Halbband 2024, 1–50 (§)

https://doi.org/10.34780/v10zrk37

Herausgebende Institution / Publisher:
Deutsches Archäologisches Institut

IMPRESSUM

Archäologischer Anzeiger
erscheint seit 1889/*published since 1889*

AA 2024/2 • 294 Seiten/*pages* mit/*with* 255 Abbildungen/*illustrations*

Herausgeber/*Editors*
Friederike Fless • Philipp von Rummel
Deutsches Archäologisches Institut
Zentrale
Podbielskiallee 69–71
14195 Berlin
Deutschland
www.dainst.org

Peer Review
Alle für den Archäologischen Anzeiger eingereichten Beiträge werden einem doppelblinden Peer-Review-Verfahren durch internationale Fachgutachterinnen und -gutachter unterzogen./*All articles submitted to the Archäologischer Anzeiger are reviewed by international experts in a double-blind peer review process.*

Redaktion und Layout/*Editing and Typesetting*
Gesamtverantwortliche Redaktion/*Publishing editor*:
Deutsches Archäologisches Institut, Redaktion der Zentralen Wissenschaftlichen Dienste, Berlin
(https://www.dainst.org/standort/zentrale/redaktion), redaktion.zentrale@dainst.de
Für Manuskripteinreichungen siehe/*For manuscript submission, see*: https://publications.dainst.org/journals/index.php/aa/about/submissions
Redaktionelle Bearbeitung/*Editing*: Dorothee Fillies, Berlin
Satz/*Typesetting*: le-tex publishing services GmbH, Leipzig
Corporate Design, Layoutgestaltung/*Layout design*: LMK Büro für Kommunikationsdesign, Berlin

Umschlagfoto/*Cover illustration*: Pontische Amphora des Paris-Malers, Inv. 55.7. The Metropolitan Museum of Art (https://www.metmuseum.org/art/collection/search/254814), Bearbeitung: Ausschnitt des Originalbildes und Verwendung eines Farbfilters, CC0 (https://creativecommons.org/publicdomain/zero/1.0/)
Gestaltung Catrin Gerlach nach Vorlage von Tanja Lemke-Mahdavi. Alle Rechte vorbehalten

Druckausgabe/*Printed edition*

Druck und Vertrieb/*Printing and Distribution*: Dr. Ludwig Reichert Verlag, Tauernstraße 11, 65199 Wiesbaden •
info@reichert-verlag.de, www.reichert-verlag.de

P-ISSN: 0003-8105 – ISBN: 978-3-7520-0835-7

Druck und Bindung in Deutschland/*Printed and bound in Germany*

Digitale Ausgabe/*Digital edition*

Webdesign/*Webdesign*: LMK Büro für Kommunikationsdesign, Berlin
XML-Export, Konvertierung/*XML-Export, Conversion*: digital publishing competence, München
Programmiertechnische Anpassung des Viewers/*Viewer Customization*: LEAN BAKERY, München

E-ISSN: 2510-4713 – DOI: https://doi.org/10.34780/wh9cv954
Zu den Nutzungsbedingungen siehe/*For the terms of use see* https://publications.dainst.org/journals/index/termsOfUse

ABSTRACT

From Earth to Eternity

Investigating Bitumen and Clay Use in Byzantine Church Construction at Ashdod-Yam

Marta Lorenzon – Lucía Ruano Posada – Myrsini Gkouma – Liora Bouzaglou – Philip Ebeling – Alexander Fantalkin

This paper presents the results of an archaeometric analysis examining bitumen and plastic earthen materials (PEM) samples brought to light at the Ashdod-Yam Byzantine church (Israel). The site, active from the late 4th or early 5th century C.E., shows evident signs of destruction by fire towards the end of the 6th century C.E. This destruction was evident from the large number of shattered roof tiles embedded in a hard, earthen matrix, suspected to be composed of clay and bitumen. Selected samples from this destruction layer underwent examination through pXRF, WD-XRF, ESEM and thin-section petrographic analyses (TSPA). The goal was to determine the composition of the roofing material through cost-effective archaeometric techniques, investigate its microstructures, and discern the manufacturing technologies employed. While clay use in roofs is well-documented in Byzantine-period structures in the region, bitumen application as an intermediate layer between tiles and ceiling has not been previously recorded, thus offering a new insight into construction practices.

KEYWORDS

Late Antique, southern Levant, ancient architecture, archaeometry, building archaeology, roofing material, bitumen

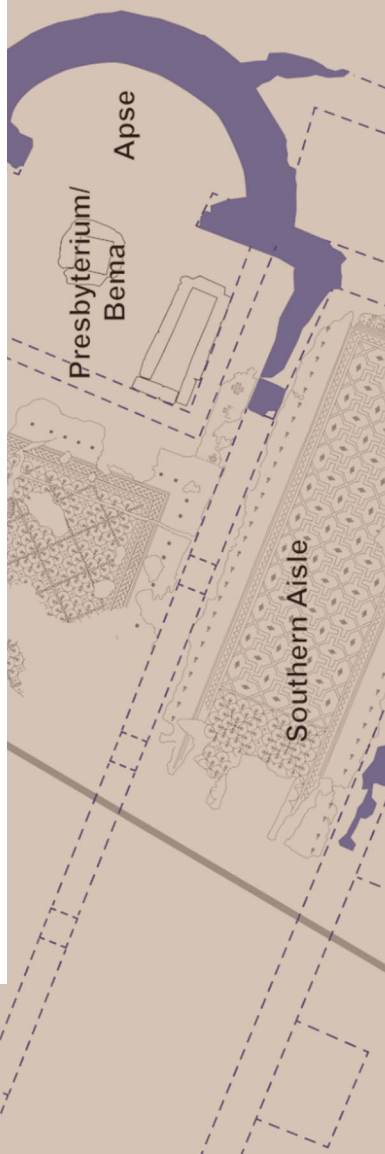

MARTA LORENZON – LUCÍA RUANO POSADA – MYRSINI GKOUMA –
LIORA BOUZAGLOU – PHILIP EBELING – ALEXANDER FANTALKIN

From Earth to Eternity

Investigating Bitumen and Clay Use in Byzantine Church Construction at Ashdod-Yam

Introduction

1 The evolution of architectural practices has often been intertwined with the exploration and adaptation of building materials that are both locally available and economically sustainable. In this context, our research delves into the innovative utilization of bitumen in connection with earthen building materials in Byzantine-period roof structures in the Southern Levant. Bitumen is a fossil hydrocarbon with high molecular weight that was extensively utilized in the ancient Fertile Crescent.[1] Bitumen can be identified in archaeological materials using gas chromatography and isotope analysis. However, this study introduces cost-effective analytical methods, not only to detect bitumen's presence, but also to discern its architectural function within an archaeological setting. As a building material, bitumen is versatile, resilient, and offers unique benefits that extend beyond traditional applications, especially when used in conjunction with earthen architecture.[2] Plastic Earthen Material (PEM) is an earthen building material compositionally similar to mud mortar, but distinguished by the deliberate inclusion of vegetal temper. This temper improves plasticity and is employed for use as a structural architectural filling. As a result, PEM often resembles mud plaster in composition – another form of earthen building material that also includes vegetal temper. However, while mud plaster is typically used as a finishing layer on walls, PEM serves a structural purpose. Both bitumen and PEM are well-known for their adhesive properties, impermeability, and their overall impact on the durability and longevity of multi-material assemblies. These qualities made them suitable for specific construction purposes in antiquity, where they were available in abundance.[3] This general statement however holds especially true for the Bronze and Iron Age periods in Western Asia where they were used for various building purposes; occasionally for roofing.[4]

1 Connan et al. 2006; Connan – Carter 2007; Connan – Deschesne 2007; Connan 2011.
2 Connan – Deschesne 1992; Lorenzon et al. 2024a.
3 Abraham 1918; Connan 1999; Connan – Van de Velde 2010.
4 Forbes 1936; Griffith et al. 2013.

2 The use of bitumen in the Mediterranean during the Hellenistic, Roman, and Byzantine periods was primarily confined to medicine and magic. Ancient recipes for various treatments using bitumen are documented.[5] However, the archaeological record provides scant evidence of its use. Ancient textual sources such as Vitruvius (De Architectura, 1.5.8) and Pliny (Naturalis Historia, 35.178–181) indicate that bitumen as a construction material in the Near East was known in Italy during the Roman Imperial period. Pliny also mentions construction with bitumen in Agrigentum, Sicily (Naturalis Historia, 35.179), yet archaeological evidence from Agrigentum itself and from throughout Sicily is absent. Similarly, the archaeological record from the Hellenistic and Roman Imperial periods in the Southern Levant seldom shows bitumen usage, except in a few cases involving minor, isolated objects.[6]

3 Greek and Roman sources occasionally describe the use of various burning, oily substances in warfare. During the Late Roman and Early Byzantine periods, sources gave more focused attention to bitumen, particularly in its military applications. This period also shows a slight resurgence in architectural use of bitumen in the Southern Levant, as evidenced by scattered instances.[7] Following the Muslim conquest of the Southern Levant in the 7th century C.E., bitumen gained greater significance, particularly in the feared ›Greek Fire‹ – a distilled derivative of liquid bitumen; highly flammable and predominantly used in warfare.[8] Potential evidence of ›Greek Fire‹ can be inferred from the ›grenades‹ – clay balls filled with a bituminous substance – found in a 10th century C.E. shipwreck.[9] However, there is no direct evidence of a fire caused by ›Greek Fire‹.

4 The limited source of bitumen in the broader Mediterranean region is attributed to the scarcity of suitable sources, as most asphalt sources were located along the southern Euphrates River, which was under Arsacid and later Sassanian control. Nonetheless, the Dead Sea also served as a source for bitumen, where materials occasionally surfaced and were collected, as noted for example by Diodorus Siculus (Bibliotheca Historica, 19.73–101). Therefore, bituminous material remnants in the Southern Levant are not rare,[10] and its presence and trade in the coastal southern Levant's Iron Age have been documented.[11] Despite this, the use of bitumen in construction at such a late date as that found in Ashdod-Yam remains unusual.

5 Following this line of inquiry, the archaeological site of Ashdod-Yam presents a compelling case study. This site displays a long history of occupation with extensive Iron Age and Roman remains, and its importance continued into the Byzantine period when it served as a religious center. The church uncovered by the Tel Aviv University excavation was active from the late 4th or early 5th century C.E.[12] The monumental public structure showcased clear signs of fire destruction at the end of the 6th century C.E., evidenced by numerous shattered roof tiles embedded in a hard debris matrix composed of mortar and plaster, bitumen and clay deriving from the collapsed roof.

6 In this framework, we employed a range of archaeometric techniques including pXRF (and WD-XRF), ESEM, thin-section petrographic analyses (TSPA) and micromorphology to investigate ceiling construction practices, particularly the combined use of clay and bitumen. Through this approach, we aimed to explore the potential of cost-effective archaeometric techniques for identifying and analyzing bitumen in ar-

5 For a compilation of sources, see Forbes 1936, 90–92.
6 Gutfeld – Rogovski 2021.
7 Atrash 2009; Atrash 2010; Hadas 2013; Atrash – Mazor 2021, 86; Tchekhanovets 2022, 320.
8 Forbes 1936, 95–100.
9 Parker 1992, 314 no. 821.
10 Oren – Scheftelowitz 1999; Hadas 2013.
11 Connan et al. 1998; Connan et al. 2006.
12 Di Segni et al. 2022; Habas 2023.

chaeological samples, as opposed to traditionally-employed methods such as Gas Chromatography coupled to Mass Spectrometry and $\delta^{13}C$ Isotope Ratio Mass Spectrometry.

Archaeological Context: The Byzantine Church of Ashdod-Yam

7 The Ashdod-Yam archaeological site, known as Ashdod-by-the-Sea, is situated on Israel's southern coast (Fig. 1). The site is encompassed by the urban sprawl of Ashdod's southern district, yet it retains the status of a protected archaeological zone. Notably, in its southern sector the site features a mound, or acropolis, enclosed within a man-made barrier. This fortification dates back to the Iron Age IIB–IIC (8th –7th centuries B.C.E.) and was also occupied during the Hellenistic period.[13] North of this enclosure lie the Roman-Byzantine city remnants, now obscured by sand dunes.

8 During Late Antiquity, a period marking the settlement activity's zenith, the Ashdod-Yam site exhibited considerable expansion, stretching approximately 2 km from north to south and around 1.5 km from east to west, as outlined by Bäbler and Fantalkin.[14] Consequently, during the Byzantine era, the coastal city of *Azotos Paralios* rose in prominence, even surpassing its inland counterpart, historically recognized in classical texts as *Azotos Hippenos* or *Azotos Mesogaios*.[15] This shift in urban significance is corroborated by the 6th century C.E. Madaba mosaic map and various historical records.[16]

9 In 2013, a new excavation initiative started at Ashdod-Yam, conducted by the Institute of Archaeology at Tel Aviv University and led by Alexander Fantalkin. In August 2017, the third season of archaeological research on the Ashdod-Yam acropolis saw the initiation of an excavation approximately 1 km northeast of the acropolis and 350–400 m eastward from the coastline. This newly targeted area (Area L) was situated amidst modern Ashdod's residential villas. The initial excavation here (permit G-78/2017) provided promising evidence of a Byzantine church, including a nearly-intact Greek dedicatory inscription and fragments of another. Subsequent extensive excavations in July–August 2019 and July 2021 (permits G-50/2019; G-26/2021) aimed at uncovering the full extent of the church complex and its associated structures.

10 These efforts led to the discovery of a sizeable basilica-style church featuring three aisles and decorative mosaic floors, alongside an ornate chapel and additional facilities. Regrettably, unregu-

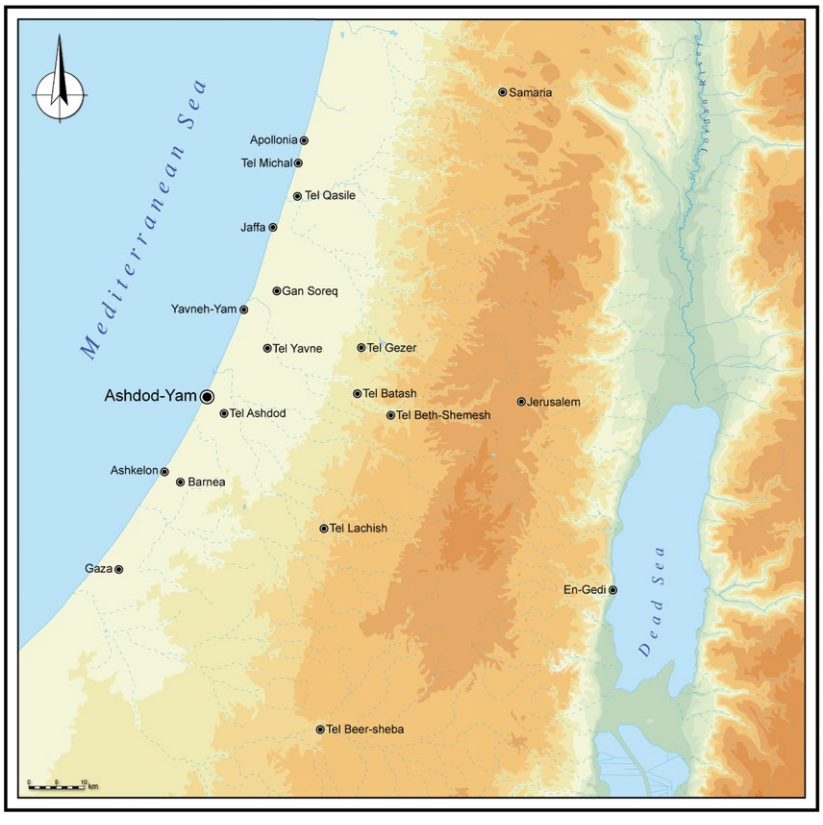

Fig. 1: Ashdod-Yam, map of the southern Levant with the location of Ashdod-Yam

1

13 Kaplan 1969; Fantalkin 2014; Fantalkin et al. 2016; Fantalkin 2018; Ashkenazi – Fantalkin 2019; Fantalkin et al. 2024a; Fantalkin et al. 2024b.

14 Bäbler – Fantalkin 2023.

15 Tsafrir et al. 1994, 72.

16 Tsafrir et al. 1994, 72.

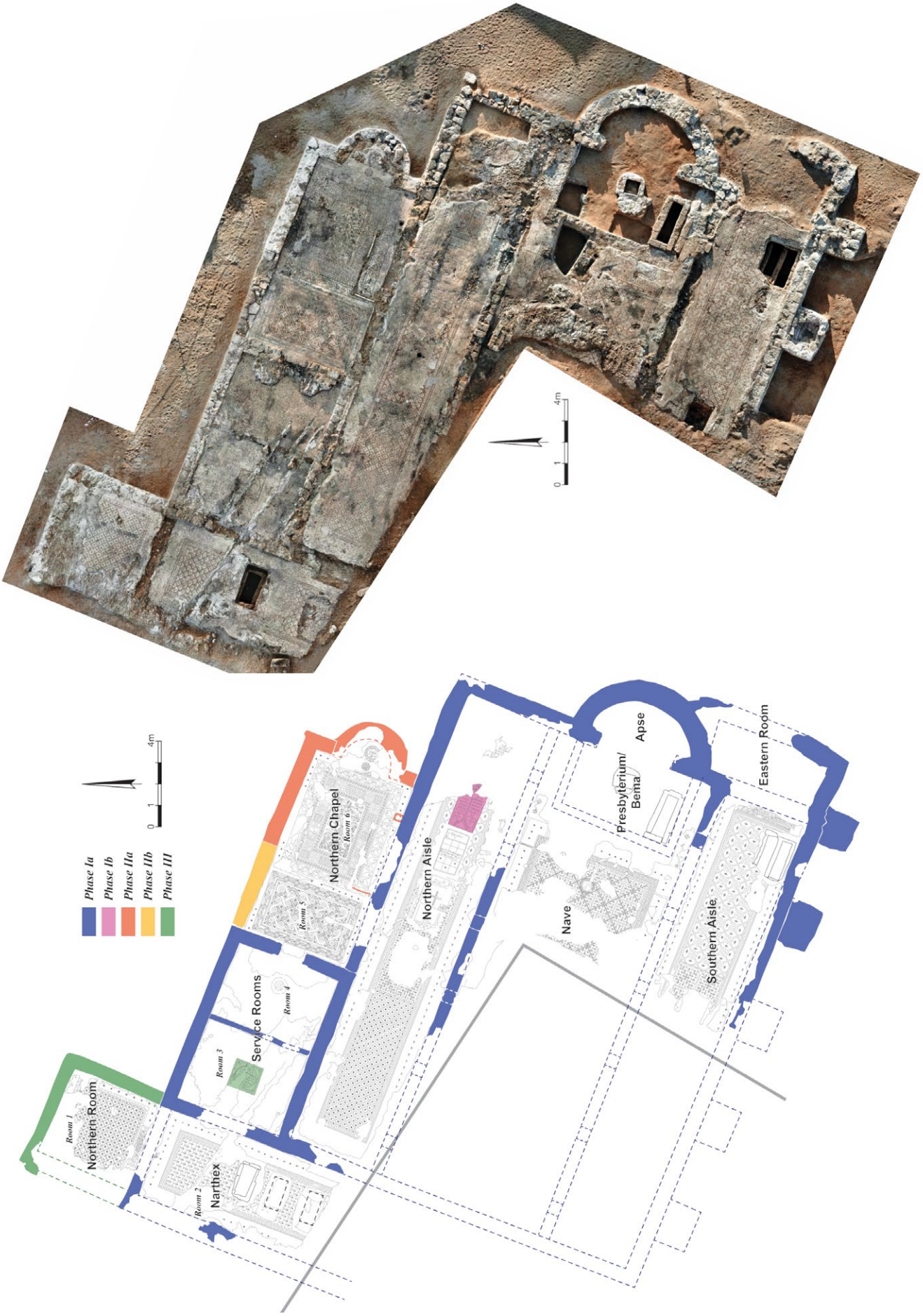

2

Fig. 2: Orthophotograph and plan of the Byzantine church at Ashdod-Yam with the mosaics floors

lated construction activities in the 1980s inflicted considerable damage on the complex's southwestern section (Fig. 2). The exposure of the church's mosaic floors revealed numerous inscriptions. These served as temporal markers, highlighting the building's architectural evolution.[17]

11 The edifice consists of a basilica c. 25 m in length and 19 m in width, aligned predominantly along an east-west axis. Its layout includes a broad nave partitioned by two pillar rows, culminating in a presbyterium/bema and an expansive semi-circular apse. The nave is bordered by two aisles, with the northern aisle extending into a chapel that features a small semi-circular apse. A spacious narthex spans the complex's western front, leading to protruding rooms at its northern edge. Each room was adorned with intricate mosaic floors.[18] Including the section destroyed by modern construction, the church spans c. 570 sqm. Numerous tombs, including some holding multiple individuals, were discovered beneath the mosaic floors respectively of the chapel's apse, the northern and southern aisles, and the narthex. The epigraphic and numismatic evidence collectively suggests the edifice's active period spanned from the late 4th or early 5th century C.E. until around 600 C.E. Every exposed section of the structure exhibited clear signs of fire damage. The majority of the debris, consisting predominantly of roof tiles, was likely part of the former roof. These fragments were found embedded in the debris, scattered throughout the church, and even outside, dispersed among the sand dunes. Chemical and mineralogical analyses indicated that the roof tiles were imported from the northeastern Mediterranean and the Judean Hills.[19] Arranged in overlapping rows, they formed a waterproof barrier, primarily secured with lime mortar, also known for its waterproof properties. Lime mortar, found in layers or as loose chunks ranging from hand-sized to microscopic particles, was prevalent throughout the destruction debris.

Bitumen Remains

12 We collected seven samples from various excavation areas of the church, with clear attestation of bitumen and other remains on top of the mosaic floors. Four samples (AY-43 to AY-46; Fig. 3. 4) were collected from the collapse debris and the conflagration layer on top of the mosaic floor in the western section of Room 5, in the church's northern annex (Locus 21). This layer is characterized by a clayish soil mixed with lime, a large amount of ash and whitish concretions. Regarding the finds, a significant quantity of roof tiles was recovered, along with several metal fragments. Near Room 5's entrance a metal key was discovered, as well as a ferrule or rod handle, an iron fitting or fastener, possibly used for building or furniture, and iron nails. This area was deemed suitable for sampling (AY-45, AY-46). Beneath this layer the mosaic floor was severely burnt, displaying black soot.

13 A sample (AY-48) was collected from an accumulation of hardened sand in Room 6 (Locus 25). Nearby, another sample (AY-49) was obtained from superstructure debris resulting from its collapse, and a burnt layer, both linked to the church's destruction (Locus 33). The debris was exceptionally well-preserved in this specific area, featuring identifiable and nearly-intact roof tiles embedded in a burnt black matrix mixed with lime and concretions. Among the finds were coins, plaster, glass fragments, and various metal objects. Additionally, marble fragments, including part of a grate, were discovered near the mosaic floor but not directly on it.

17 Di Segni et al. 2022.

18 Habas 2023.

19 Ebeling et al. forthcoming.

ID	Type	Basket	Locus	Description	Location	Inclusions
AY-43	Roof	B.1061	L. 21	Conflagration Square E11	Northern Annex Room 5, west	+
AY-44	Floor (?) possibly mixed with ceiling	B.1063	L. 21	Conflagration Square E11	Northern Annex Room 5, west	++
AY-45	PEM	B.1075	L. 21	Conflagration Square E11	Northern Annex Room 5, west	++
AY-46	PEM	B.1076	L. 21	Conflagration Square E11	Northern Annex Room 5, west	++
AY-47	Roof	B.1142	L. 71	Conflagration Square C10	Central Narthex Room 2	+++
AY-48	Roof (?)	B.1143	L. 25	Accumulation above collapse F11	Northern Annex Room 6, northeast	++
AY-49	PEM	B.1144	L. 33	Conflagration Square F11	Northern Annex Room 6, northeast	++

3

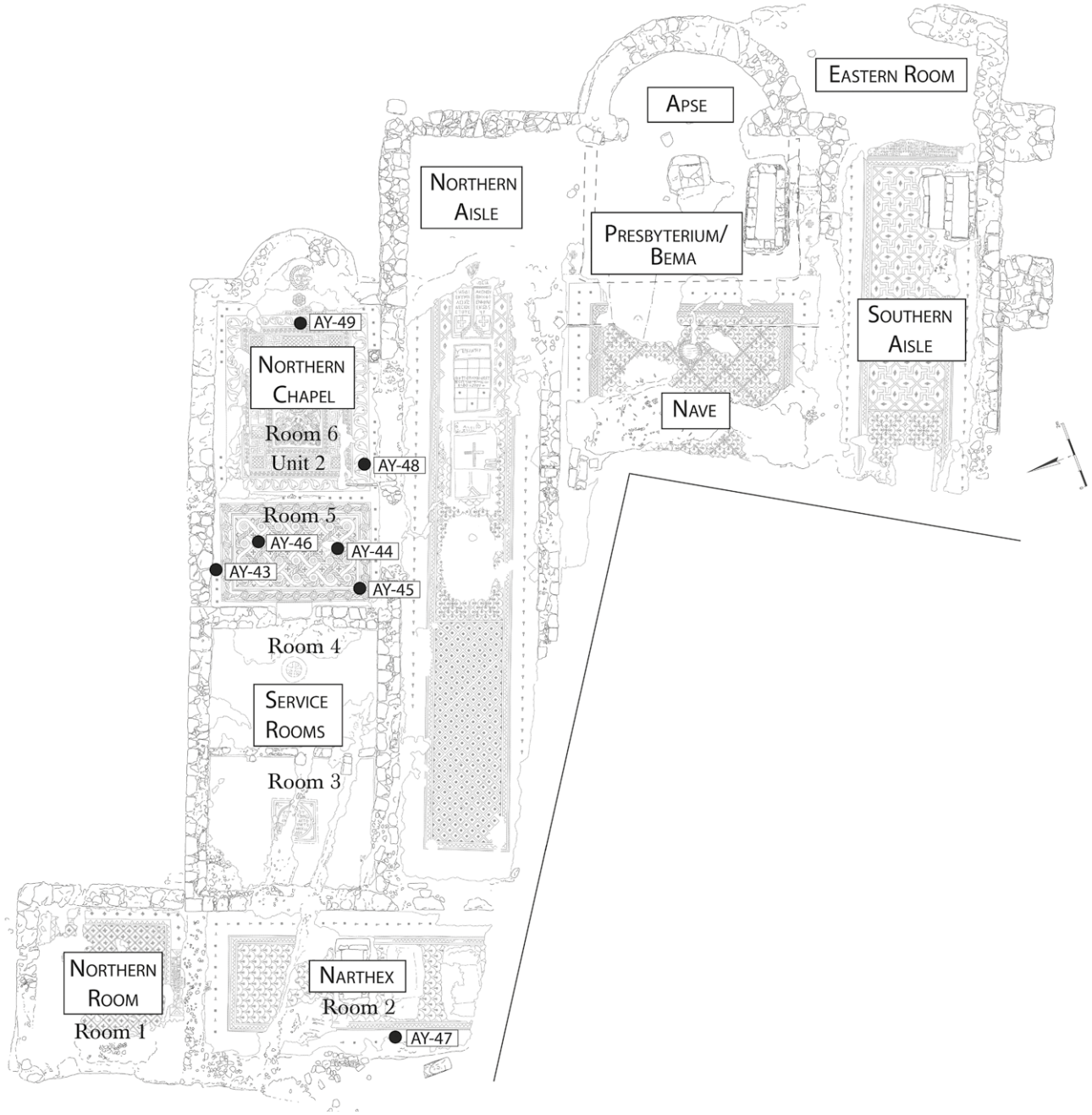

4

Fig. 3: Table of macroscopic description and location of the samples from within the Byzantine church at Ashdod-Yam

Fig. 4: Byzantine church plan with the location of samples analyzed

14 A last sample was collected from the destruction layer in Room 2, located in the narthex (AY-47 in Locus 71). Viewed from above, the destruction pattern in this area resembled waves, akin to hardened viscous substances, similar to cold lava flows. The pottery covered by this layer on the mosaic floor appeared melted and severely overheated. Clay begins to melt in temperatures between 1250–1400° C, depending on the components. Such high temperatures can only have been reached by the presence of flux. Due to these observations the presence of bitumen was suspected, as it melts at about 200–220° C and burns long and hot once ignited, particularly when combined with wood (Fig. 5).[20]

5

Fig. 5: The destruction debris during the excavations of the nave in Unit 2 from the Byzantine church at Ashdod-Yam

Methods

15 The decision to utilize pXRF was based on its non-destructive nature, emphasizing the importance of preserving the limited sample quantity for further micromorphological analysis. Elemental analysis was carried out using the Bruker S1 TITAN handheld XRF set to mining mode, with the resulting data presented in Fig. 6. The pXRF parameters include a 4 W, 50 kV tantalum anode X-Ray tube and a high-performance Silicon Drift Detector (SDD) enveloped in graphene. This detector possesses a resolution of 145 eV (Mo-Kα), shielded by a 20-mm window. In light of the material constraints, each sample underwent three measurements, each lasting 180 seconds. As a result, the values documented in Fig. 6 represent the mean outcomes derived from three successive runs. The results of these analyses were statistically analyzed through both triangular scattergram and principal component analysis (PCA) using R software (version 4.3.1). The data were normalized prior to analysis.

16 A limited number of samples were re-analyzed with a Rigaku NEX-DE VS bench-top ED-XRF spectrometer. The analyses were conducted in a helium atmosphere, employing tube voltages of 60 kV, 35 kV, and 6.5 kV for high-Z, mid-Z, and low-Z elements, while the acquisition times were 60, 60, and 100 seconds for high-Z, mid-Z, and low-Z elements. We also employed WD-XRF for a better definition of a few light elements present, but also to test and evaluate the feasibility of using pXRF for the correct identification of elemental compounds in diverse building materials.[21]

17 The samples also underwent examination using an environmental scanning electron microscope (ESEM- FEI Quanta 200FEG) operating in high vacuum mode. The instrument, equipped with an Everhart-Thonley Secondary Electron (SE) detector, was operated at the Faculty of Engineering at Tel Aviv University and calibrated using standard samples provided by the manufacturer.[22]

18 Petrographic and micromorphological analyses were employed to examine the detailed physical and geological characteristics of the samples. For this study, thin sections of the seven samples were prepared and investigated using a Leica DM2000 polarized light microscope fitted with a digital camera, operating within a magnification range of × 5 to × 40. The samples were examined and categorized based on the description of soil and pottery thin sections.[23]

20 Schwartz – Hollander 2000.

21 Lorenzon et al. 2024b.

22 Ashkenazi – Fantalkin 2019.

23 Bullock et al. 1985; Whitbread 1989; Whitbread 1995; Quinn 2013.

Sample	MgO	Al_2O_3	SiO_2	P_2O_5	S	Cl	K_2O	CaO	Ti
AY-43	2,7451	3,1621	21,4267	0,2815	0,1932	0,0498	0,2472	16,0182	0,2545
AY-44	2,5247	3,8453	25,5573	0,2188	0,1666	0,0523	0,2963	18,6169	0,2668
AY-45	1,9953	3,5605	23,6424	0,2032	0,2921	0,0479	0,3547	14,5354	0,2824
AY-46	2,0591	3,9835	26,3118	0,1375	0,0783	0,0361	0,4202	10,2862	0,3304
AY-47	1,6867	5,4478	35,3647	0,0752	0,0068	0,0137	0,5418	5,1380	0,3361
AY-48	1,9566	9,6129	47,5063	0,2662	0,0472	0,0454	0,8840	16,3610	0,5886
AY-49	2,2056	3,4137	22,4043	0,1152	0,0621	0,0301	0,2694	10,3744	0,2734

Sample	V	Cr	Mn	Fe	Ni	Cu	Zn	As	Rb
AY-43	0,0018	0,0000	0,0220	1,1145	0,0016	0,0035	0,0016	0,0004	0,0017
AY-44	0,0013	0,0007	0,0249	1,4534	0,0011	0,0037	0,0014	0,0005	0,0022
AY-45	0,0015	0,0000	0,0244	2,7184	0,0013	0,0033	0,0015	0,0014	0,0018
AY-46	0,0000	0,0000	0,0294	1,8991	0,0019	0,0033	0,0024	0,0008	0,0025
AY-47	0,0015	0,0000	0,0255	1,4217	0,0020	0,0025	0,0019	0,0003	0,0020
AY-48	0,0009	0,0027	0,0588	3,1006	0,0028	0,0047	0,0028	0,0015	0,0021
AY-49	0,0019	0,0000	0,0235	1,2703	0,0015	0,0033	0,0018	0,0009	0,0016

Sample	Sr	Y	Zr	Nb	Mo	Ag	Sn	Ba	Pb
AY-43	0,0382	0,0007	0,0187	0,0002	0,0000	0,0000	0,0000	0,0080	0,0031
AY-44	0,0191	0,0011	0,0154	0,0004	0,0000	0,0000	0,0000	0,0127	0,0092
AY-45	0,0170	0,0010	0,0146	0,0000	0,0000	0,0000	0,0000	0,0000	0,0105
AY-46	0,0173	0,0014	0,0185	0,0008	0,0004	0,0000	0,0038	0,0080	0,0079
AY-47	0,0106	0,0009	0,0155	0,0005	0,0000	0,0000	0,0036	0,0073	0,0000
AY-48	0,0318	0,0018	0,0294	0,0007	0,0002	0,0011	0,0000	0,0359	0,0091
AY-49	0,0297	0,0008	0,0171	0,0000	0,0000	0,0000	0,0000	0,0000	0,0026

Fig. 6: Table with pXRF results of the seven analyzed Ashdod-Yam samples

6

19 Soil micromorphological samples were oven-dried at 50° C and then impregnated using a 9:1 mixture of polyester resin with acetone and 1 % catalyst. Precut sample slabs measuring 5 cm × 7 cm were processed to thin sections of 30 µm thickness. Flatbed scanning or static high-resolution images of whole thin sections were used to observe features at the mesoscale.[24] The thin sections were studied using a polarizing microscope at various magnifications (× 12.5, 20, 40, 50, 100 and 400). Micromorphological descriptions follow the terminology of Courty et al.[25] and Stoops.[26]

Results

Chemistry

20 The data from the pXRF geochemical analysis are presented in Fig. 6 (Appendix A), encompassing values for 27 elements and compounds (MgO, Al_2O_3, SiO_2, P_2O_5, S, Cl, K_2O, CaO, Ti, V, Cr, Mn, Fe, Ni, Cu, Zn, As, Rb, Sr, Zr, Nb, Mo, Ag, Sn, Ba, and Pb). These

24 Carpentier – Vandermeulen 2016.
25 Courty et al. 1989.
26 Stoops 2020.

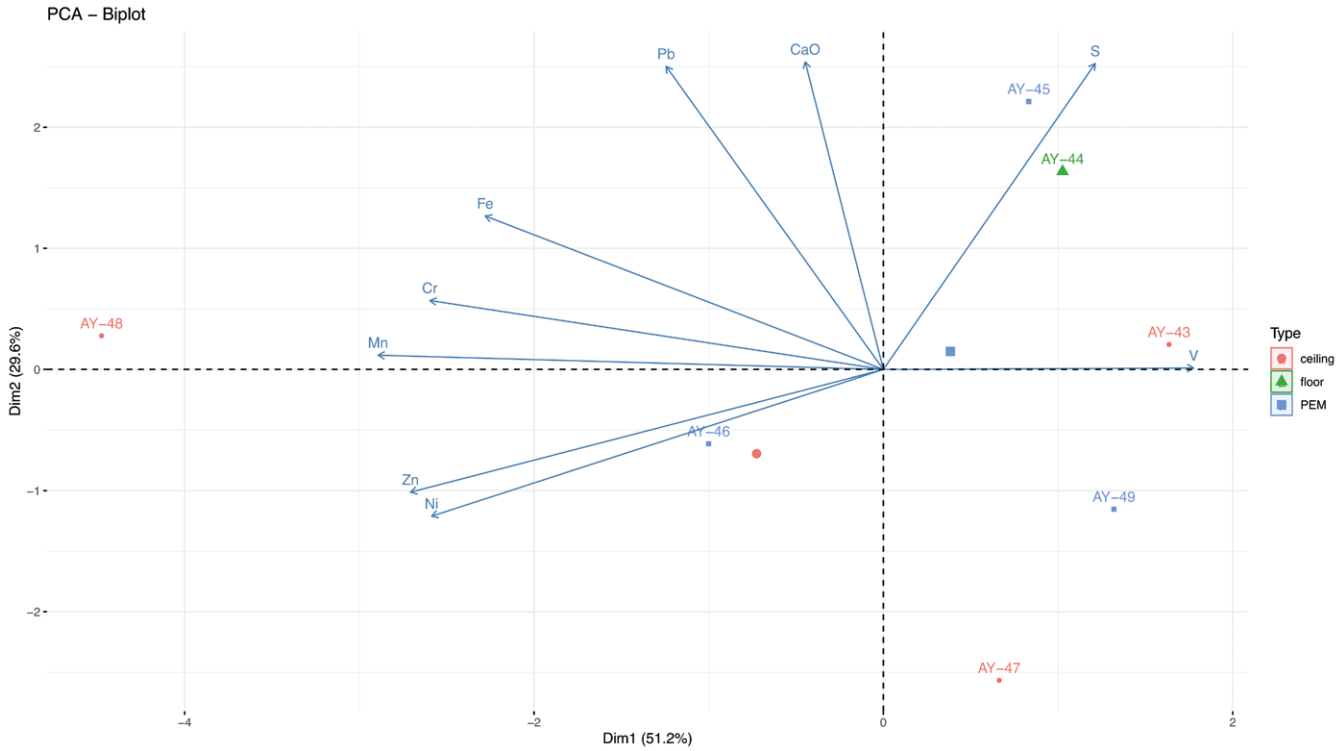

7

Fig. 7: Principal component analysis (PCA) created using S, CaO, Cr, Mn, Fe, Ni, Zn, Pb as variables. R software (version 4.3.1)

particular elements were chosen due to their reliability in pXRF analysis, demonstrating minimal error margins.[27]

21 Additionally, it should be noted that some of these elements serve as proxies for bitumen (e. g. Ni, S, V, Cr, and Fe).[28] The two principal components, PC1 and PC2, collectively account for 80.8 % of the overall variability (respectively 51.2 % and 29.6 %).

22 The PCA, conducted with elements associated with crude oil, reveals no clear groupings, suggesting significant variability among the samples (Fig. 7); however, the point distribution provides us with additional information to help characterize the samples. Sample AY-48 stands out as a clear outlier, indicating a significantly different geochemical fingerprint when compared to the other samples. AY-48 is characterized by a high percentage of Mn and Fe, which corresponds in its high clay content, as seen in petrographic analyses. Samples AY-44 and AY-45 deviate slightly from the main cluster due to the presence of S in their chemical fingerprint. Samples AY-43, AY-44, AY-47, and AY-49 are marked by a higher value of V.

23 To complement and verify the findings from the PCA, we created two triangular scattergrams to analyze the composition of our samples further, selecting two sets of elements relevant to bitumen detection. We selected the elements Vanadium (V), Nickel (Ni), and Manganese (Mn) due to their relevance in analyzing bitumen and clay materials. Bitumen often contains elevated concentrations of V and Ni, while Mn serves as a comparative baseline for clay materials. This first scattergram (Fig. 8) reveals that samples AY-44, AY-45, AY-49, and AY-43 are clustered near the vertex representing Vanadium, suggesting elevated V levels in these samples. This finding aligns with the PCA results, where these samples also showed higher V concentrations, potentially indicating the presence of bitumen or related organic traces. Sample AY-47 is positioned along the line between V and Ni, which suggests a more moderate presence of V in this

27 Goodale et al. 2012; Hunt – Speakman 2015.

28 Lu et al. 2018; Ni et al. 2020.

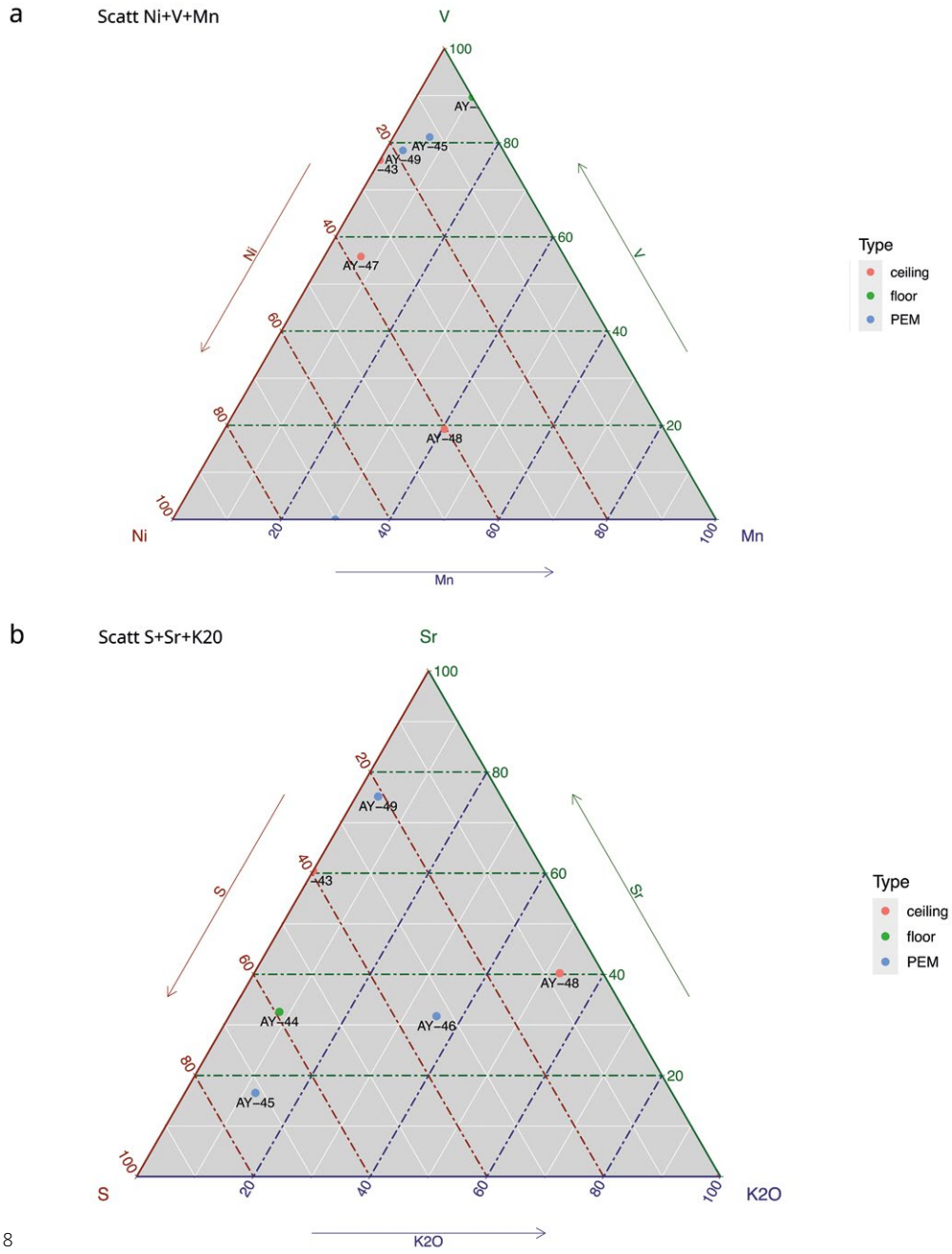

Fig. 8: Triangular scattergrams clustering a: V, Ni and Mn, b: Sr, S and K_2O. R software (version 4.3.1)

Fig. 9: Table with the EDXRF results from Ashdod-Yam samples AY 44 and AY 47

	Na_2O	MgO	Al_2O_3	SiO_2	P_2O_5	SO_3	Cl	K_2O	CaO	TiO_2	V_2O_5	Cr_2O_3	MnO	Fe_2O_3
	mass%	mass%	mass%	mass%	mass%	mass%	mass%	mass%	mass%	mass%	mass%	mass%	mass%	mass%
AY 44	0	12,510	107,482	575,390	0,5324	0,4228	0,0504	16,098	188,047	18,895	0,0537	0,0244	0,1193	67,670
Std dev.	0	0,0133	0,1024	0,3661	0,0011	0,0150	0,0006	0,1516	0,3637	0,0168	0,0344	0,0136	0,0068	0,0142
AY 47	21,460	12,497	103,253	609,539	0,5862	0,4062	0,0486	15,187	172,808	12,235	0,0364	0,0160	0,1134	53,919
Std dev	0,0000	0,0435	0,0907	0,5172	0,0176	0,0191	0,0010	0,1325	0,5214	0,0200	0,0328	0,0000	0,0065	0,1551

	NiO	CuO	ZnO	As_2O_3	Br	Rb_2O	SrO	Y_2O_3	ZrO_2	BaO	Ga	Co_2O_3	Nb	Pb
	mass%	mass%	mass%	mass%	mass%	mass%	mass%	mass%	mass%	mass%	mass%	mass%	mass%	mass%
AY 44	0,0028	0,0044	0,0080	0,0024	0,0022	0,0062	0,0393	0,0048	0,0766	0,0350	0,0009	0,0045	0,0039	0,0094
Std dev.	0,0020	0,0020	0,0015	0,0006	0,0005	0,0008	0,0013	0,0006	0,0004	0,0022	0,0006	0,0049	0,0000	0,0005
AY 47	0,0049	0,0059	0,0056	0,0013	0,0009	0,0048	0,0334	0,0044	0,0574	0,0252	0,0010	0,0055	0,0021	0,0021
Std dev	0,0000	0,0000	0,0015	0,0018	0,0003	0,0004	0,0012	0,0012	0,0047	0,0020	0,0001	0,0049	0,0000	0,0003

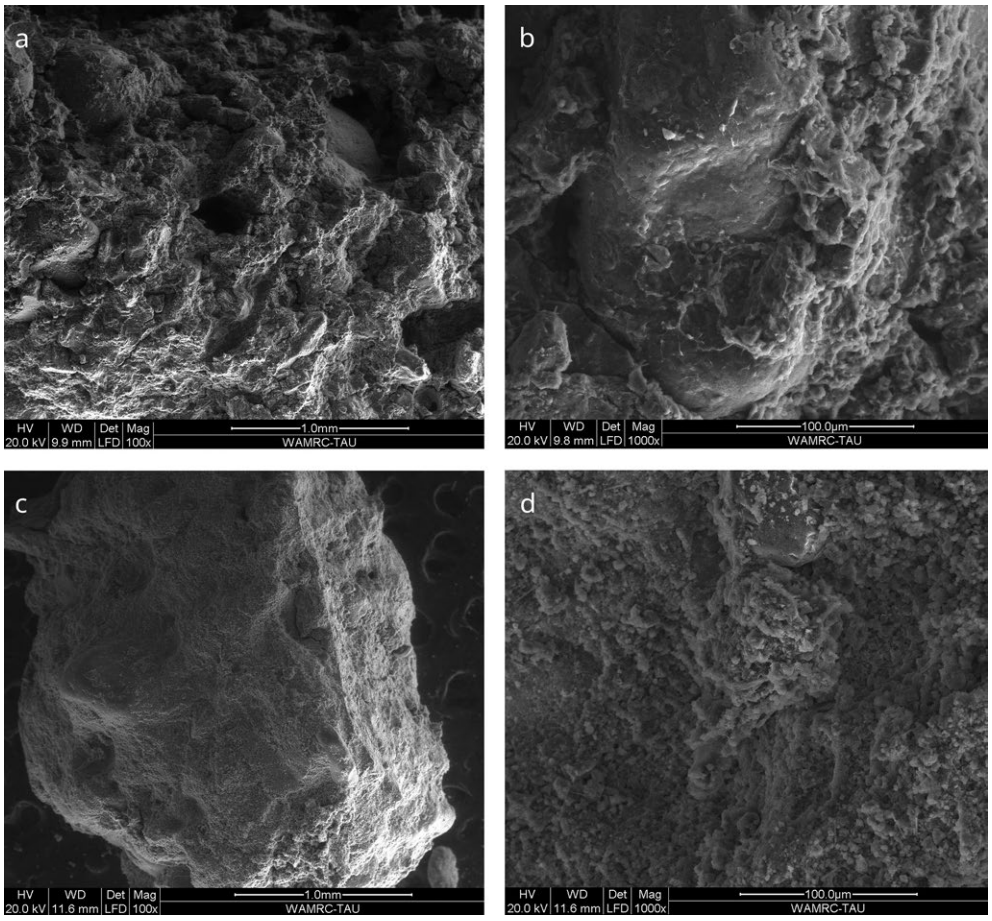

Fig. 10: SEM images from samples a and b: AY-47; c and d: AY-44

10

sample compared to the others. Conversely, sample AY-48 is separated from this cluster, confirming its status as outlier and suggesting a distinct geochemical profile.

24 The second scattergram focuses on the elements Strontium (Sr), Sulfur (S), and Potassium Oxide (K_2O), each of which provides critical insights into the material compositions (Fig. 8). Sulfur is a strong indicator of bitumen, given its common presence in its composition, while Sr and K_2O reflect the characteristics of the clay matrix. Sr also serves as a proxy for carbonate content. Elevated S levels relative to Sr and K_2O suggest the presence of bitumen in a sample.

25 In this diagram, sample AY-49 is positioned closer to the Sr vertex along the S-Sr axis, indicating relatively low sulfur content. AY-43 occupies a more central position along this axis, reflecting a balance between S and Sr. Samples AY-44 and AY-45 are slightly closer to the S vertex, suggesting minor sulfur enrichment that could indicate traces of bitumen. Sample AY-46 is located near the center of the triangle, suggesting balanced levels of Sr, S, and K_2O.

26 In contrast, samples AY-48 and AY-47 are positioned near the K_2O vertex, highlighting a composition distinct from the other samples. This distribution reveals a preliminary grouping: AY-43, AY-44, and AY-45 cluster toward the S vertex, indicating significant mixing with bitumen. Meanwhile, AY-49 and AY-46, with lower levels of clay minerals, K_2O, and Sr, stand apart from this group.[29]

27 Samples AY-44 and AY-47 were then selected to be re-analyzed through WD-XRF (Appendix B); then with ESEM (Appendix C); and analyzed to ascertain the levels of Vanadium (V) and any eventual variability with pXRF. V is often used as an indicator element for bitumen or heavy crude oil, but its analysis through pXRF may be unreli-

29 Morgenstein – Redmount 2005; IARC 2013.

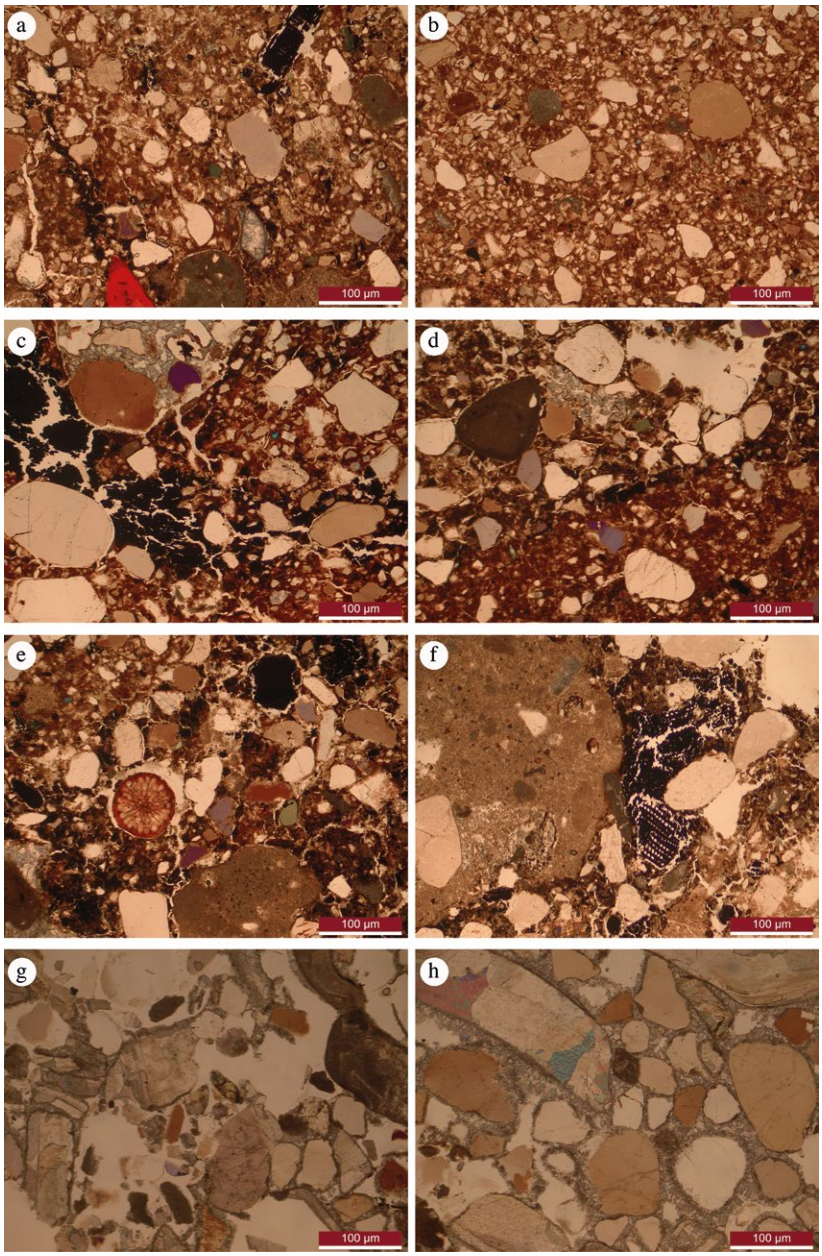

11

Fig. 11: Photomicrographs of petro-groups identified in Ashdod-Yam samples, plane polarized light (PPL). Fabric 1, a: AY-43, b: AY-48, c: AY-46, d: AY-47, and e–f: AY-44; Fabric 2, g–h: AY-49

able. Both samples, however, did indicate the presence of V in combination with Ni and Cr; elements also often associated with crude oils, and thus supporting the pXRF results (Fig. 9).

28 We further investigated Samples AY-44 and AY-47 through ESEM (Fig. 10). The results highlight the consistent presence of bitumen, as indicated by the worm structure identified in both samples (Lu et al. 2018). Alongside bitumen, Sample AY-44 has visible quartz contents, while Sample AY-47 presents evidence of calcite crystals.

Thin-Section Petrographic Analyses

29 The TSPA of the samples allows us to identify different fabrics, depending on the characteristics of the groundmass and the type, size, and distribution of the inclusions.[30]

30 Fabric 1 (n = 6) is composed by a reddish-brown active matrix and a heterogeneous distribution of inclusions (c.f.v. 30:60:10 – 45:50:5) (Fig. 11 a–f). It displays a bimodal distribution pattern, characterized by a densely-packed fine fraction (c. 0.001 mm, very fine silt), with close-spaced and moderately-sorted inclusions. The coarse fraction (c. 0.1–0.5 mm, very fine sand to coarse sand) presents a single- to open-spaced distribution of poorly-sorted sub-rounded and sub-angular grains. The more common inclusions are monocrystalline quartz, while less common ones consist of clay pellets, mudstone, feldspars, microcline, pumice, and iron oxides. Rare limestone, clinopyroxene and biotite grains are also visible. Bitumen is observed in several samples (see AY-43, AY-44, AY-45, AY-46, and AY-47; Fig. 11 a. c. d. e).

31 Voids are present in all the samples, generally shaped as vughs and channels; possibly related to stress cracking and to shrinking (Fig. 11 c. e). They appear to be randomly distributed. Embedded into the matrix, we recognized fragments of bivalve shells (some of large size, >1 mm); and, to a lesser extent, different types of microfossils, such as echinoids (AY-44; Fig. 11 e); and planktonic and benthic foraminifera, such as globigerinoides (AY-47). Most samples from this fabric also attested charcoal, some of which retained their microstructure (see AY-43, AY-44, or AY-45; Fig. 11 a. f), providing further evidence of the conflagration event that destroyed the building.

32 The quantity and distribution of inclusions, as well as the presence of various intercalations in the samples, enable us to distinguish between two different sub-fab-

30 See Quinn 2013 for the methodology.

rics. Sub-fabric 1.1 (n = 1) includes Sample AY-48, which exhibits the aforementioned features but showcases a prevalent homogeneous fine fraction and a low percentage of inclusion (Fig. 11 b). Bitumen has not been detected in this sample. Sub-fabric 1.2 (n = 5) exhibits similar qualitative features, but also a high percentage of inclusions, specifically monocrystalline quartz (AY-43, AY-44, AY-45, AY-46, and AY-4). In addition, bitumen is clearly noticeable in all the samples belonging to this fabric (Fig. 11 a. c. d. e). Sample AY-47 also features a lime plaster fragment embedded in the matrix.

33 Fabric 2 (n = 1) was only identified for Sample AY-49 (Fig. 11 g. h), which exhibits a calcitic matrix with abundant poorly distributed inclusions (c.f.v. 40:40:20). These show a bimodal pattern between fine silt and medium sand (0.01–0.4 mm), mainly composed of quartz and calcite grains. To a lesser extent, grains of clinopyroxenes, schists, microcline, mudstone, and clay pellets were identified. Voids are quite common, typically taking the form of macro- and meso-vughs and channels, with a random orientation.

Soil Micromorphology

34 Soil micromorphological analysis was carried out on samples large enough for the study, including Samples AY-43, AY-44, AY-45, AY-46, and AY-47.

Sample AY-43

35 The sediments include loamy sands with sand-sized rounded to sub-rounded quartz (0.5 mm size) and dispersed calcareous nodules incorporating quartz sand grains (Fig. 12 a. b. d), plagioclase feldspar and calcite. The matrix exhibits a reddish-brown color and contains 10 % elongated shell fragments, each up to 0.5 cm in size, altered by diagenetic processes[31] (Fig. 12 a. c). They are characterized by crude laminated distribution.

36 Abundant angular, elongated charcoal fragments (10 %) less than 1 cm size were identified, along with organic remains of sub-angular shape (Fig. 12 a), which preserve fiber needles.

37 SEM analysis reveals a cellular microstructure, but it does not allow for the identification of the specific type or part of the plant from which these structures originate. The b/f fabric is crystallitic, which along with the presence of charcoal remains, indicates the addition of ashes in the matrix.

38 The deformation features are limited and ill-developed with abundant poly-concave vughs. The microstructure is massive, with a few elongated channels occasionally curvilinear, which indicate mild compaction processes.[32]

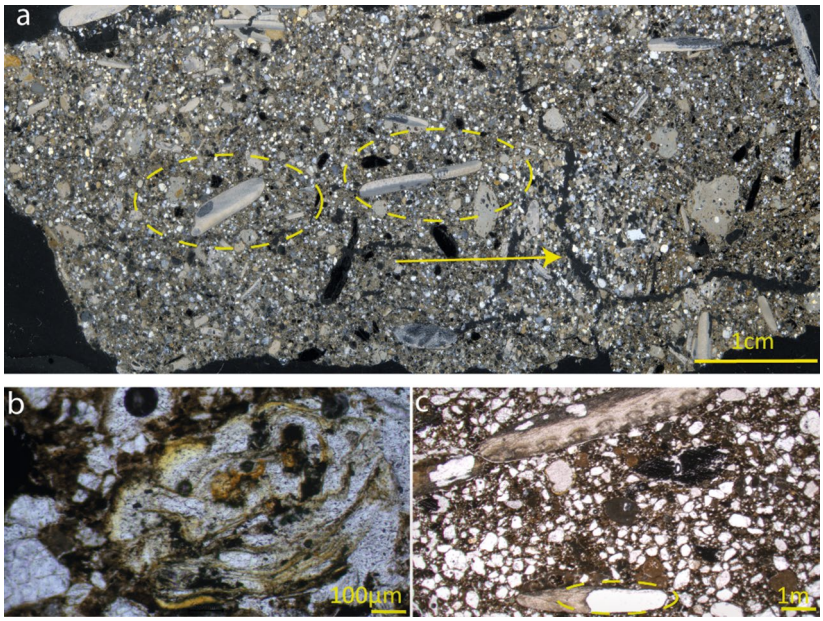

Fig. 12: a: Flat-scanned thin sections of sample AY-43 in XPL, showing curvilinear fracture (arrow) and randomly distributed shells (circles); b: photomicrograph of sub-rounded organic features in PPL; c: photomicrograph of altered part of shells (in circle) due to diagenetic processes (PPL)

Sample AY-44

39 Poorly-sorted sandy-silt loams, with predominantly sand-sized quartz and shells, as well as abundant charcoal fragments of less than 1 cm size are recorded. The sample's lower half shows sub-angular aggregates of reddish-brown silty clay loams (Fig. 13). Rounded organic

12

31 Karkanas – Goldberg 2019, 85.

32 Rentzel et al. 2017.

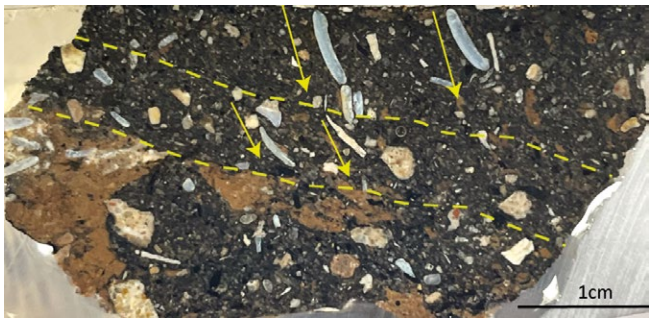

13

Fig. 13: Polished resin-impregnated slab of sample AY-44, showing bands of shells with ›tiled‹ arrangement (arrows) oriented transverse to the shear zone indicated in yellow dotted lines

nodules are also preserved, as described above. Vughs and voids are very limited and randomly distributed, indicating mild compression and a limited amount of water applied in the sediments.[33] Planar shear zones are designated by shells with a »tiled« arrangement transverse to the shear surface (Fig. 13). They appear to represent the direction of compression and deceleration as the pressure subsided and slid to a halt.[34] The reddish-brown sediments may represent a lower shear surface. Overall, the construction appears to have been executed in three distinct phases, as shown in Fig. 13.

Sample AY-45

40 The sediments include loamy sands with sand-sized quartz, rounded to sub-rounded – 0.5 mm – and dispersed calcareous nodules incorporating quartz sand grains (Fig. 14 a. b. d), plagioclase feldspar, and calcite. They are poorly sorted, with a few but sizeable elongated shell fragments randomly distributed along with charcoal fragments. Vughs are few and rounded, randomly distributed, and oriented in an otherwise massive microstructure indicating mild compaction.[35] Many rounded organic inclusions and fiber needles are confirmed through SEM. Queras, noted as evidence of sediment exposure, are pedofeatures created by the impregnation of root tissues close to the surface, commonly seen in semi-arid soils.[36] In this instance, they manifest as channel fillings composed of coarse cytomorphic calcite.

Sample AY-46

41 The sample is divided in two sedimentary units: upper (1) composed of moderately-sorted reddish-brown silty clay loams and lower (2) composed of dark-gray sandy loams (Fig. 15 a. b). Unit 1 is massive in microstructure with few planar voids indicating repeated compaction,[37] forming fissility due to the plastering process of a watery slurry. Rounded organic inclusions and infillings of phytomorphic calcite (Fig. 15 d) are also recorded (queras); which, as already noted, indicate exposure of the sediments. The lower part (2) has vertical small channels, due to more intensive compaction; it is coarser in composition and more calcareous; b/f fabric is crystallitic including many aggregates of recrystallized ashes (10 %) and abundant (30–40 %) charcoal fragments of c. 1 cm size. The undulating boundary between the units along with the vertical intrusions of Unit 1 in Unit 2 (Fig. 15 a) indicate the watery composition of the sediments.

Sample AY-47

42 The sample includes light grayish-white sandy loams with a reddish-brown silty clay loam intercalation of 1 cm thickness (Fig. 16). Charred remains and pelloids from calcareous rock fragment dissolution are included. Crystallitic fillings from ash recrystallization are also present. Fine vertical channels due to compaction, and numerous parallel linear and wavy fine voids are abundant, as well as arrays of vesicles, produced by repeated application of mud slurries.[38] Separations have been formed along microlayers. Fine laminations of bitumen form surfaces applied in several layers. The undulating deformation indicates the watery composition of the sediments.

33 Karkanas 2019.
34 Karkanas 2019.
35 Rentzel et al. 2017.
36 Yousefifard et al. 2015.
37 Karkanas 2019.
38 Karkanas 2019.

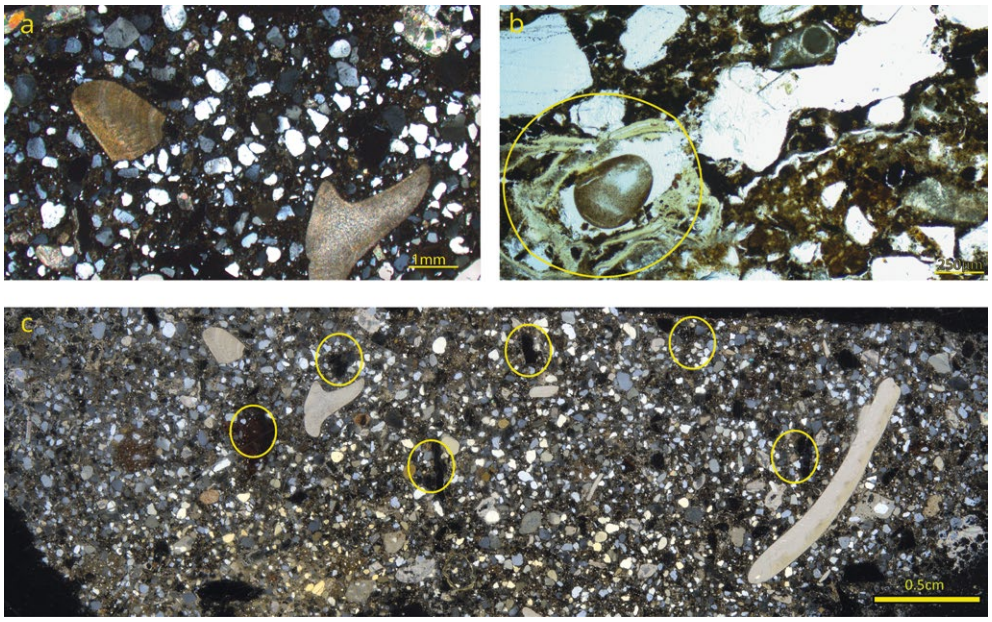

14

Fig. 14: a: Photomicrograph of sample AY-45 with coarse-grained sand-sized quartz and shell fragments (XPL); b: photomicrograph of reddish-brown loams with organic features in a circle; c: flat-scanned thin section with ill-developed deformation features in the form of small and randomly distributed vughs (circles)

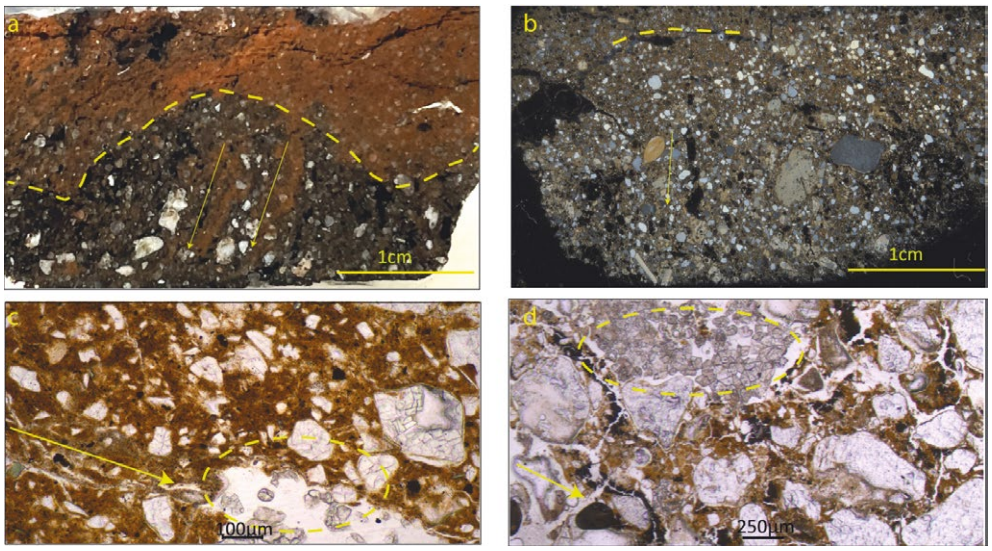

15

Fig. 15: a: Polished resin-impregnated slab of sample AY-46, where the wavy boundary separating the two sedimentary layers is marked by a dotted line. Vertical intrusions (indicated by arrows) from the upper sedimentary unit into the lower indicate the presence of a watery slurry; b: flat-scanned thin section in XPL. Note upper part characterized by massive microstructure with fine planar channels forming fissility due to the plastering process of a watery slurry. Fissility may be caused by water that develops pathways through the sediment, leading to interconnected shear planes accommodating both deformation of the sediment and evacuation of water. This interpretation is probably valid for some linear arrangements of fine planar voids observed in resurfaced occupational debris and during wet brooming (Karkanas 2019). The lower unit is characterized by vertical channels due to moderate compaction; c: photomicrograph of sample AY-46 (b), where fine planar channels are indicated with an arrow and infillings with coarse phytomorphic calcite (queras) shown in circle (PPL); d: bitumen (arrow) and fillings of phytomorphic calcite (circle) (PPL)

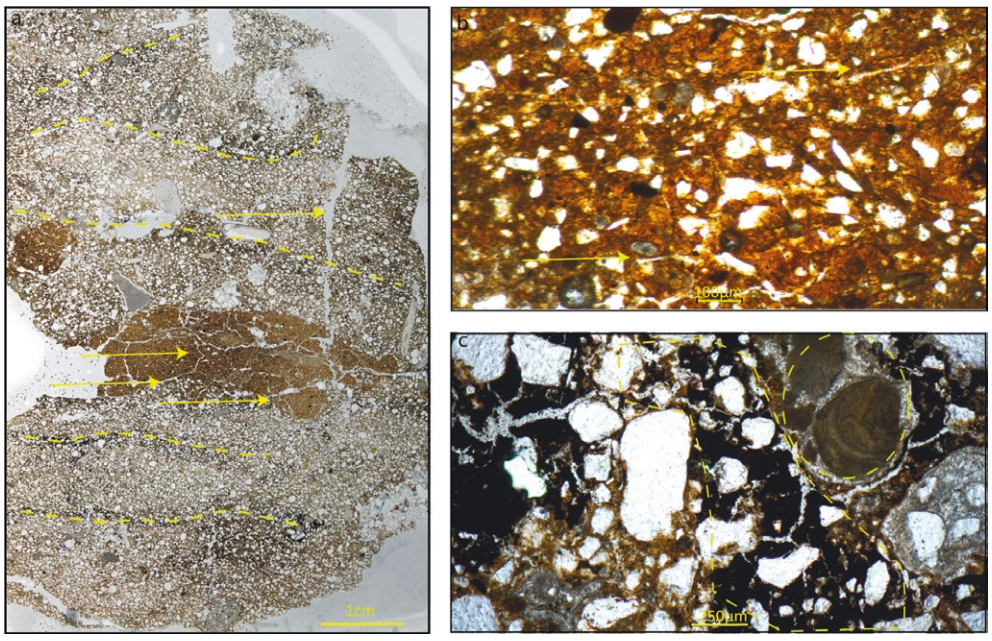

16

Fig. 16: a: Flat-scanned thin section of sample AY-47 in XPL, displaying vertically-oriented planar voids (crudely curvilinear) linked to fine planar channels, demonstrating fissility. These features are marked with arrows. Undulating laminations of organic charred remains are shown in yellow dotted lines; b: photomicrograph of fine planar channels (arrows) (PPL); c: bitumen indicated in yellow irregular shape (XPL). Shown in the circle are pelloids originating from the calcareous sandstone nodules

Discussion

43 Our analyses highlight the composite nature of the roof, in which multiple building materials were present. As suspected while excavating, the results of this study confirmed the presence of bitumen within the roof debris in Samples AY-43, AY-44, AY-45, AY-47, and AY-49, while it is notably absent in Samples AY-46 and AY-48. The samples containing bitumen originate with certainty from the collapsed roof structure, showcasing a mixture of bitumen and clay, likely resulted in the degradation of PEM used in the roofing structure. The mixture may indicate a post-depositional process or pre-depositional process.

44 Bitumen's absence in Samples AY-46 and AY-48 suggests several possibilities: the analyzed substances may not have originated from the roof, parts of the roof could have been constructed without bitumen, or the samples could have come from areas of the roof not in direct contact with bitumen. However, the presence of charcoal in Sample AY-46 indicates it was contemporaneous with the destruction, and not deposited long afterward.

45 Architecturally, the use of bituminous material in the roof structure was appropriate given its properties. It was likely applied as a mastic, its most common application,[39] as suggested by evidence from the church itself. This mastic was intended to serve as a water sealant to prevent leaks, rather than as an adhesive. The mastic mixture included alongside bitumen also PEM, made of loamy clay – materials readily available near Ashdod, and used for pottery and sun-dried brick production since the Iron Age.[40] Additionally, vegetal temper was identified in Sample AY-43's composition. Both PEM and vegetal matter are components in similar bituminous mastics detected in Bronze and Iron Age period structures (both private and monumental) found in Mesopotamia and further eastwards. These examples often include additional ingredients like sand and gravel, which were likely also used in Ashdod-Yam. Thus, we can infer that the mastic recipe used in Ashdod-Yam was not significantly different from those used centuries earlier in Mesopotamia. The nearest bitumen source is in Dead Sea deposits, which have been harvested, utilized, and exported since prehistoric times.[41] This proximate source might have been utilized for Ashdod-Yam, and further analyses will confirm this hypothesis.

46 The presence of different components in construction recipes with bitumen can provide us with relevant information about early operational technical chains. Thus, the different ways of working with this raw material not only speak to us about its different origins and formats but also about how each human group may have had its own way of dealing with bitumen, depending on their knowledge, other available materials, and perhaps also its intended specific use. The methodology of analysis presented here, grounded in comprehensive chemical, petrological, and micromorphological examinations, holds significant potential not only for identifying the bitumen's presence in construction samples but also for providing insights into the various ways it was employed. While the limited number of samples in this case study constrains our ability to propose diverse construction recipes, they do underscore the substantial potential this integrated approach holds for enhancing our understanding of construction in the Byzantine world, and offers a potentially efficient and financially feasible application for other periods and regions as well.

47 In conclusion, the use of analytical methods such as pXRF, ESEM, and micromorphology has confirmed the presence of bitumen in various samples from the

39 Forbes 1936; Connan 1999.

40 Lorenzon et al. 2024a.

41 Oron et al. 2015; Fulcher et al. 2020.

collapsed church roof. The correlation observed between the presence of bitumen and concentrations of chemical elements such as vanadium, sulfur and manganese show the potential for using field techniques such as pXRF to conduct elemental analysis as a tool for bitumen characterization. An initial characterization can then be confirmed by more comprehensive laboratory analysis.

48 Moreover, the utilization of diverse methodologies, such as the combined approach of pXRF, ESEM, and micromorphology, proves to be efficient in the characterization of bitumen in archaeological contexts. This study thus highlights the efficiency of employing more affordable techniques, including portable ones in the field, now proven capable of detecting the presence of bitumen. This may lead to a more refined sampling strategy and then to further inquiries into issues related to its production and application processes.

49 Furthermore, this application of bitumen represents a previously undocumented technique for the Byzantine period in the wider region. The bitumen was probably used for waterproofing the roof, together with other more common and more readily available materials. The absence of bitumen in other samples could hint at a varied use across the structure, perhaps not directly involving the sealant. The association of bitumen with these architectural remains and its apparent key role in the construction recipe offers new insights on ancient construction techniques.

Availability of Measurement Data

50 The Measurement Data of the analyzed Ashdod-Yam samples is available in the data repository iDAI.repo (https://doi.org/10.34780/dy7eff02):

- Appendix A: data from the pXRF geochemical analysis (cf. Fig. 6)
- Appendix B: Samples AY-44 and AY-47 re-analyzed through WD-XRF
- Appendix C: Samples AY-44 and AY-47 re-analyzed with ESEM

List of Abbreviations

ESEM	Environmental Scanning Electron Microscope
PCA	Principal Component Analysis
PEM	Plastic Earthen Materials
PPL	Plane Polarized Light
pXRF	Portable X-Ray Fluorescence
SDD	Silicon Drift Detector
TSPA	Thin-Section Petrographic Analyses
WD-XRF	Wavelength-Dispersive X-Ray Fluorescence
XPL	Crossed Polarized Light

References

Abraham 1918 H. Abraham, Asphalts and Allied Substances. Their Occurrence, Modes of Production, Uses in the Arts and Methods of Testing (New York 1918)

Ashkenazi – Fantalkin 2019 D. Ashkenazi – A. Fantalkin, Archaeometallurgical and Archaeological Investigation of Hellenistic Metal Objects from Ashdod-Yam (Israel), Archaeological and Anthropological Sciences 11, 2019, 913–935, https://doi.org/10.1007/s12520-017-0579-1

Atrash 2009 W. Atrash, Bet She'an (West). Preliminary Report, Hadashot Arkheologiyot. Excavations and Surveys in Israel 121, 2009, https://www.hadashot-esi.org.il/report_detail_eng.aspx?id=1308&mag_id=115 (01.05.2024)

Atrash 2010 W. Atrash, Mesillot. Final Report, Hadashot Arkheologiyot. Excavations and Surveys in Israel 122, 2010, https://www.hadashot-esi.org.il/report_detail_eng.aspx?id=1402&mag_id=117 (01.05.2024)

Atrash – Mazor 2021 W. Atrash – G. Mazor, Remains from the Hellenistic – Early Islamic Periods at Horbat Tarbenet, Atiqot 104, 2021, 75–100

Bäbler – Fantalkin 2023 B. Bäbler – A. Fantalkin, Azotos Paralios during the Periods of Roman and Byzantine Domination. Literary Sources vs. Archaeological Evidence, in C. Horn – B. Bäbler (eds.), Word and Space Interacting in Palestine in Late Antiquity. Towards a History of Pluridimensionality, Eastern Mediterranean Texts and Contexts 5, (Chesterfield, Missouri 2023) 89–119

Bullock et al. 1985 P. Bullock – N. Fedoroff – A. Jongerius – G. Stoops – T. Tursina, Handbook for Soil Thin Section Description (Albrighton 1985)

Carpentier – Vandermeulen 2016 F. Carpentier – B. Vandermeulen, High-Resolution Photography for Soil Micromorphology Slide Documentation, Geoarchaeology 31, 2016, 603–607, https://doi.org/10.1002/gea.21563

Connan 1999 J. Connan, Use and Trade of Bitumen in Antiquity and Prehistory. Molecular Archaeology Reveals Secrets of Past Civilizations, Philosophical Transactions of the Royal Society of London. Series B: Biological Sciences, 354 (1379), 1999, 33–50, https://doi.org/10.1098/rstb.1999.0358

Connan 2011 J. Connan, Les mélanges bitumineux du Tell d'Akkaz (Koweït). The Bituminous Mixtures from Tell Akkaz (Kuwait), in: J. Gachet-Bizollon (ed.), Le Tell d'Akkaz au Koweit/Tell Akkaz in Kuwait, Travaux de la Maison de l'Orient 57, Chapitre 15 (Lyon 2011) 339–412

Connan – Carter 2007 J. Connan – R. Carter, A Geochemical Study of Bituminous Mixtures from Failaka and Umm an-Namel (Kuwait), from the Early Dilmun to the Early Islamic Period, ArabAEpigr 18, 2007, 139–181, https://doi.org/10.1111/j.1600-0471.2007.00283.x

Connan – Deschesne 1992 J. Connan – O. Deschesne, Archaeological Bitumen: Identification, Origins and Uses of an Ancient Near Eastern Material, MRS Online Proceedings Library (OPL) 267, 1992, 683, https://doi.org/10.1557/PROC-267-683

Connan – Deschesne 2007 J. Connan – O. Deschesne, Le bitume à Mari, in: J. C. Margueron – O. Rouault – P. Lombard (eds.), Akh Purratim, Série Akh Purattim – Les rives de l'Euphrate. Mémoires d'archéologie et d'histoire interdisciplinaires, Maison de l'Orient et de la Méditerranée – Ministère des affaires étrangères (Lyon 2007) 165–206, https://doi.org/10.4000/books.momeditions.3848

Connan – Van de Velde 2010 J. Connan – T. Van de Velde, An Overview of Bitumen Trade in the Near East from the Neolithic (c. 8000 BC) to the Early Islamic Period, ArabAEpigr 21, 2010, 1–19, https://doi.org/10.1111/j.1600-0471.2009.00321.x

Connan et al. 1998 J. Connan – P. Lombard – R. Killick – F. Hojlund – J. F. Salles – A. Khala, The Archaeological Bitumens of Bahrain from the Early Dilmun Period (c. 2200 BC) to the Sixteen Century AD. A Problem of Sources and Trade, ArabAEpigr 9, 1998, 141–181, https://doi.org/10.1111/j.1600-0471.1998.tb00116.x

Connan et al. 2006 J. Connan – A. Nissenbaum – K. Imbus – J. Zumberge – S. Macko, Asphalt in Iron Age Excavations from the Philistine Tel Miqne-Ekron City (Israel): Origin and Trade Routes, Organic Geochemistry 37, 2006, 1768–1786, https://doi.org/10.1016/j.orggeochem.2006.08.015

Courty et al. 1989 M. A. Courty – P. Goldberg – R. Macphail, Soils and Micromorphology in Archaeology (Cambridge 1989), https://doi.org/10.1097/00010694-199012000-00014

Di Segni et al. 2022 L. Di Segni – L. Bouzaglou – A. Fantalkin, A Recently Discovered Church at Ashdod-Yam (Azotos Paralios) in Light of Its Greek Inscriptions, StBiFranc 72, 2022, 399–447, https://doi.org/10.1484/J.LA.5.134545

Ebeling et al. forthcoming P. Ebeling – L. Bouzaglou – D. Ashkenazi – J. H. Sterba – A. Fantalkin, From the Hills to the Sea: Mineralogical and Chemical

Characterization of a Roof Tile Assemblage from the Byzantine Church at Ashdod-Yam, Advances in Archaeomaterials (forthcoming)

Fantalkin 2014 A. Fantalkin, Ashdod-Yam on the Israeli Mediterranean Coast. A First Season of Excavations, Skyllis 14, 2014, 45–57

Fantalkin 2018 A. Fantalkin, Neo-Assyrian Involvement in the Southern Coastal Plain of Israel: Old Concepts and New Interpretations, in: S. Zelig Aster – A. Faust (eds.), The Southern Levant under Assyrian Domination (Eisenbrauns 2018) 162–185

Fantalkin et al. 2016 A. Fantalkin – M. Johananoff – S. Krispin, Persian-Period Philistian Coins from Ashdod-Yam, IsrNumJ 11, 2016, 23–28

Fantalkin et al. 2024a A. Fantalkin – E. Itkin – O. Chesnut – M. Mazis – M. Lorenzon – L. Bouzaglou – T. Eshel – J. Sharvit, Iron Age Remains from Ashdod-Yam (2013–2019): An Interim Report, Journal of Eastern Mediterranean Archaeology and Heritage Studies 12, 3, 2024, 250–297, https://doi.org/10.5325/jeasmedarcherstu.12.3.0250

Fantalkin et al. 2024b A. Fantalkin – M. Mazis – Y. Schauer – D. T. Ariel – S. Krispin – O. Tsuf – T. Eshel – E. Itkin, Hellenistic Ashdod-Yam in Light of Recent Archaeological Investigations, TelAvivJA 51, 2, 2024, 238–278, https://doi.org/10.1080/03344355.2024.2385149

Forbes 1936 R. J. Forbes, Bitumen and Petroleum in Antiquity 1 (Leiden 1936), https://doi.org/10.1136/bmj.1.3934.1132-b

Fulcher et al. 2020 K. Fulcher – R. Stacey – N. Spencer, Bitumen from the Dead Sea in Early Iron Age Nubia, Scientific Reports 10, 1, 2020, 8309, https://doi.org/10.1038/s41598-020-64209-8

Goodale et al. 2012 N. Goodale – D. G. Bailey – G. T. Jones – C. Prescott – E. Scholz – N. Stagliano – C. Lewis, pXRF: A Study of Interinstrument Performance, JASc 39, 2012, 875–883, https://doi.org/10.1016/j.jas.2011.10.014

Griffith et al. 2013 G. Griffiths – R. Langridge – B. Cather – D. Doran, Bituminous Material, in: D. Doran – B. Cather (eds.), Construction Materials Reference Book (London 2013)

Gutfeld – Rogovski 2021 O. Gutfeld – T. Rogovski, The Old City of Jerusalem, Tif'eret Yisra'el Synagogue, Hadashot Arkheologiyot. Excavations and Surveys in Israel 133, 2021, https://www.hadashot-esi.org.il/report_detail_eng.aspx?id=26022&mag_id=133 (01.05.2024)

Habas 2023 L. Habas, Symbols of Faith in the Mosaic Floors of the Newly Discovered Ecclesiastical Complex at Ashdod Maritima, Israel, Journal of Mosaic Research 16, 2023, 251–267, https://doi.org/10.26658/jmr.1376813

Hadas 2013 G. Hadas, En Gedi, Hadashot Arkheologiyot. Excavations and Surveys in Israel 125, 2013, https://www.hadashot-esi.org.il/report_detail_eng.aspx?id=2287&mag_id=120 (01.05.2024)

Hunt – Speakman 2015 A. M. W. Hunt – R. J. Speakman, Portable XRF Analysis of Archaeological Sediments and Ceramics, JASc 53, 2015, 626–638, https://doi.org/10.1016/j.jas.2014.11.031

IARC 2013 IARC, Bitumens and Bitumen Emissions, and Some N- and S-Heterocyclic Polycyclic Aromatic Hydrocarbons, IARC Monographs on the Evaluation of Carcinogenic Risks to Humans 103 (Lyon 2013)

Kaplan 1969 J. Kaplan, The Stronghold of Yamani at Ashdod-Yam, IEJ 19, 1969, 137–149, https://doi.org/10.1512/iumj.1969.19.19017

Karkanas 2019 P. Karkanas, Microscopic Deformation Structures in Archaeological Contexts, Geoarchaeology 34, 2019, 15–29, https://doi.org/10.1002/gea.21709

Karkanas – Goldberg 2019 P. Karkanas – P. Goldberg, Reconstructing Archaeological Sites: Understanding the Geoarchaeological Matrix (Oxford 2019), https://doi.org/10.1002/9781119016427

Lorenzon et al. 2024a M. Lorenzon – B. Cutillas-Victoria – E. Itkin – A. Fantalkin, Masters of Mudbrick: Geoarchaeological Analysis of Iron Age Earthen Public Buildings at Ashdod-Yam (Israel), Geoarchaeology 39, 2024, 35–62, https://doi.org/10.1002/gea.21977

Lorenzon et al. 2024b M. Lorenzon – B. Cutillas-Victoria – A. Lichtenberger – O. Tal, Of Mudbrick and Stone: A Geoarchaeological View on Innovations in Building Practices at Hellenistic Tell Iẓṭabba, Journal of Archaeological Science: Reports 54, 2024, 104389, https://doi.org/10.1016/j.jasrep.2024.104389

Lu et al. 2018 X. Lu – P. Sjövall – H. Soenen – M. Andersson, Microstructures of Bitumen Observed by Environmental Scanning Electron Microscopy (ESEM) and Chemical Analysis Using Time-of-Flight Secondary Ion Mass Spectrometry (TOF-SIMS), Fuel 229, 2018, 198–208, https://doi.org/10.1016/j.fuel.2018.05.036

Morgenstein – Redmount 2005 M. Morgenstein – C. A. Redmount, Using Portable Energy Dispersive X-Ray Fluorescence (EDXRF) Analysis for On-Site Study of Ceramic Sherds at El Hibeh, Egypt, JASc 32, 2005, 1613–1623, https://doi.org/10.1016/j.jas.2005.05.004

Ni et al. 2020 Z. Ni – Z. Chen – M. Li – C. Yang – L. Wen – H. Hong – B. Luo, Trace Element Characterization of Bitumen Constraints on the Hydrocarbon Source of the Giant Gas Field in Sichuan Basin, South China, Geological Journal 55, 2020, 317–329, https://doi.org/10.1002/gj.3412

Oren – Scheftelowitz 1999 R. Oren – N. A. Scheftelowitz, Giv'at Oranim (Naḥal Bareqet), Hadashot Arkheologiyot. Excavations and Surveys in Israel 18, 1999, 48–50

Oron et al. 2015 A. Oron – E. Galili – G. Hadas – M. Klein, Early Maritime Activity on the Dead Sea: Bitumen Harvesting and the Possible Use of Reed Watercraft, Journal of Maritime Archaeology 10, 2015, 65–88, https://doi.org/10.1007/s11457-015-9135-2

Parker 1992 A. J. Parker, Ancient Shipwrecks of the Mediterranean and the Roman Provinces, BARIntSer 580 (Oxford 1992), https://doi.org/10.30861/9780860547365

Quinn 2013 P. Quinn, Ceramic Petrography: the Interpretation of Archaeological Pottery & Related Artefacts in Thin Section (Oxford 2013), https://doi.org/10.2307/j.ctv1jk0jf4

Rentzel et al. 2017 P. Rentzel – C. Nicosia – A. Gebhardt – D. Brönnimann – C. Pümpin – K. Ismail-Meyer, Trampling, Poaching and the Effect of Traffic, in: C. Nicosia – G. Stoops (eds.), Archaeological Soil and Sediment Micromorphology (Chichester 2017) 281–297, https://doi.org/10.1002/9781118941065.ch30

Schwartz – Hollander 2000 M. Schwartz – D. Hollander, Annealing, Distilling, Reheating and Recycling. Bitumen Processing in the Ancient Near East, Paléorient 26, 2, 2000, 83–91, https://doi.org/10.3406/paleo.2000.4712

Stoops 2020 G. Stoops, Guidelines for Analysis and Description of Soil and Regolith Thin Sections (Hoboken 2020), https://doi.org/10.1002/9780891189763

Tchekhanovets 2022 Y. Tchekhanovets, Excavations on the Southwestern Margins of Giv'ati Parkin Lot, Jerusalem, Atiqot 106, 2022, 303–338

Tsafrir et al. 1994 Y. Tsafrir – L. Di Segni – J. Green, Tabula Imperii Romani – Judaea Palaestina (Jerusalem 1994)

Whitbread 1989 I. K. Whitbread, The Application of Ceramic Petrology to the Study of Ancient Greek Transport Amphorae: With Special Reference to Corinthian Amphora Production (Unpublished Ph.D. Diss. University of Southampton 1989)

Whitbread 1995 I. K. Whitbread, Greek Transport Amphorae. A Petrological and Archaeological Study (Athens 1995)

Yousefifard et al. 2015 M. Yousefifard – S. Ayoubi – R. M. Poch – A. Jalalian – H. Khademi – F. Khormali, Clay Transformation and Pedogenic Calcite Formation on a Lithosequence of Igneous Rocks in Northwestern Iran, Catena 133, 2015, 186–197, https://doi.org/10.1016/j.catena.2015.05.014

ILLUSTRATION CREDITS

Title Page: Itamar Ben Ezra Source: Atlas of Israel (1956–1964). Survey of Israel and Bialik Institute (in Hebrew), cropped version of original
Fig. 1: Itamar Ben Ezra Source: Atlas of Israel (1956–1964). Survey of Israel and Bialik Institute (in Hebrew)
Fig. 2: Slava Pirsky – Sergey Alon
Fig. 3: Marta Lorenzon
Fig. 4: Slava Pirsky – Liora Bouzaglou
Fig. 5: Sasha Flit
Fig. 6: Marta Lorenzon
Fig. 7: Lucía Ruano Posada
Fig. 8: Lucía Ruano Posada
Fig. 9: Marta Lorenzon
Fig. 10: Marta Lorenzon
Fig. 11: Lucía Ruano Posada
Fig. 12: Myrsini Gkouma
Fig. 13: Myrsini Gkouma
Fig. 14: Myrsini Gkouma
Fig. 15: Myrsini Gkouma
Fig. 16: Myrsini Gkouma

CONTACT

Dr Marta Lorenzon
Department of Cultures, University of Helsinki
marta.lorenzon@helsinki.fi
ORCID-iD: https://orcid.org/0000-0003-4747-5241
ROR ID: https://ror.org/040af2s02

Dr Lucía Ruano Posada
Department of Prehistory, Ancient History and Archaeology, Complutense University of Madrid
ORCID-iD: https://orcid.org/0000-0002-0966-9136
ROR ID: https://ror.org/02p0gd045

Dr Myrsini Gkouma
Malcolm H. Wiener Laboratory for Archaeological Science, American School of Classical Studies at Athens, Athens, Greece and Science and Technology in Archaeology and Culture Research Center, The Cyprus Institute, Nicosia, Cyprus
ORCID-iD: https://orcid.org/0000-0003-0189-1629
ROR ID: https://ror.org/03638wk09

Liora Bouzaglou
Paris 1 Panthéon, Sorbonne, Paris, France (ArScAn-VEPMO UMR 7041) and Department of Archaeology and Ancient Near Eastern Cultures, Institute of Archaeology, Tel Aviv University, Ramat Aviv 6997801, Israel
liora.bouzaglou@gmail.com
ROR ID: https://ror.org/002t25c44

Philip Ebeling
Institute of Classical and Christian Archaeology, University of Münster, Germany
philip.ebeling@googlemail.com
ROR ID: https://ror.org/002t25c44

Prof Dr Alexander Fantalkin
Department of Archaeology and Ancient Near Eastern Cultures, Institute of Archaeology, Tel Aviv University, Ramat Aviv 6997801, Israel
ORCID-iD: https://orcid.org/0000-0001-5996-6465
ROR ID: https://ror.org/04mhzgx49

METADATA

Titel/*Title*: From Earth to Eternity. Investigating Bitumen and Clay Use in Byzantine Church Construction at Ashdod-Yam

Band/*Issue*: 2024/2

Bitte zitieren Sie diesen Beitrag folgenderweise/*Please cite the article as follows*: M. Lorenzon – L. R. Posada – M. Gkouma – L. Bouzaglou – Ph. Ebeling – A. Fantalkin, From Earth to Eternity. Investigating Bitumen and Clay Use in Byzantine Church Construction at Ashdod-Yam, AA 2024/2, § 1–50, https://doi.org/10.34780/v10zrk37

Online veröffentlicht am/*Online published on*: 05.05.2025

DOI: https://doi.org/10.34780/v10zrk37

Schlagwörter/*Keywords*: Late Antique, southern Levant, ancient architecture, archaeometry, building archaeology